Ethanedithiol Treatment of Solution-Processed ZnO Thin Films: Controlling the Intragap States of Electron Transporting Interlayers for Efficient and Stable Inverted Organic Photovoltaics

Sai Bai, Yizheng Jin, Xiaoyong Liang, Zhizhen Ye, Zhongwei Wu, Baoquan Sun, Zaifei Ma, Zheng Tang, Jianpu Wang, Uli Wuerfel, Feng Gao and Fengling Zhang

Original Publication:

Sai Bai, Yizheng Jin, Xiaoyong Liang, Zhizhen Ye, Zhongwei Wu, Baoquan Sun, Zaifei Ma, Zheng Tang, Jianpu Wang, Uli Wuerfel, Feng Gao and Fengling Zhang, Ethanedithiol Treatment of Solution-Processed ZnO Thin Films: Controlling the Intragap States of Electron Transporting Interlayers for Efficient and Stable Inverted Organic Photovoltaics, 2015, ADVANCED ENERGY MATERIALS, (5), 5, 1401606.
http://dx.doi.org/10.1002/aenm.201401606

Submitted to ADVANCED ENERGY MATERIALS

DOI: 10.1002/aenm.((please add manuscript number))
Article type: Full Paper

Ethanedithiol Treatment on Solution-Processed ZnO Thin Films: Controlling The Intragap States of Electron Transporting Interlayers for Efficient and Stable Inverted Organic Photovoltaics

Sai Bai,[1] Yizheng Jin,[1] Xiaoyong Liang,[1] Zhizhen Ye,[1] Zhongwei Wu,[2] Baoquan Sun,[2*] Zaifei Ma,[3] Zheng Tang,[3] Jianpu Wang,[4] Uli Würfel,[5,6] Feng Gao,[3*] and Fengling Zhang [3]*

Dr. S. Bai, Dr. Y. Jin, X. Liang, Prof. Z.Ye,
[1] State Key Laboratory of Silicon Materials, Department of Materials Science and Engineering, Cyrus Tang Center for Sensor Materials and Application, and Center for Chemistry of High-Performance and Novel Materials, Zhejiang University, Hangzhou 310027, China
E-mail: yizhengjin@zju.edu.cn
Z. Wu, Prof. B. Sun
[2] Jiangsu Key Laboratory for Carbon-Based Functional Materials & Devices, Institute of Functional Nano & Soft Materials (FUNSOM), Soochow University,
199 Ren'ai Road, Suzhou 215123, China
E-mail:bqsun@suda.edu.cn
Dr. Z. Ma, Dr. Z. Tang, Dr. F. Gao, Dr. F. Zhang3
[3] Department of Physics, Chemistry and Biology (IFM), Linköping University, SE-581 83 Linköping, Sweden
E-mail:fengga@ifm.liu.se
Prof. J. Wang
[4] Institute of Advanced Materials, Nanjing Tech University, Nanjing 210009, China
Dr. U. Würfel
[5] Fraunhofer Institute for Solar Energy Systems ISE, Heidenhofstr. 2, 79110 Freiburg, Germany
Dr. U. Würfel
[6] Materials Research Centre FMF, University of Freiburg,
Stefan-Meier-Str. 21, 79104 Freiburg, Germany

Keywords: organic solar cells, ZnO thin film, electron transporting interlayers, intragap states, molecular passivation

Abstract

The surface defects of solution-processed ZnO films lead to various intragap states. When the solution-processed ZnO films are used as electron transport interlayers (ETLs) in inverted organic solar cells, the intragap states act as interfacial recombination centers for photogenerated charges and thereby degrade the device performance. Here we demonstrate a simple surface-passivation method based on ethanedithiol (EDT) treatment, which effectively removes the surface defects of the ZnO nanocrystal films by forming zinc ethanedithiolates. The surface passivation by EDT treatment modulates the intragap states of the ZnO films and introduces a new intragap band. When the EDT treated ZnO nanocrystal films are used as ETLs in inverted organic solar cells, both the power conversion efficiency and stability of the devices are improved. Our control studies show that the solar cells with EDT treated ZnO films exhibit reduced charge recombination rates and enhanced charge extraction properties. These features are consistent with the fact that the modulation of the intragap states results in reduction of interfacial recombination as well as the improved charge selectivity and electron transport properties of the ETLs. We further demonstrate that the EDT treatment based passivation method can be extended to ZnO films deposited form Sol-gel precursors. Our study provide an excellent example that advances on the surface chemistry, together with new understanding on the electronic properties of interfacial materials are critical for improving the performance of organic solar cells.

1. Introduction

Bulk heterojunction organic photovoltaics (OPVs) are attractive for low-cost energy harvesting due to the possibility of employing high throughput solution-processable fabrication techniques and the compatibility with large-area and flexible plastic substrates.[1-4] OPVs with an inverted structure have been proposed to improve the long-term stability.[5,6] In this device configuration, the bottom transparent electrodes are modified by interlayers with low work function, serving as electron-transporting interlayers (ETLs).[7-10] ZnO is an attractive material for ETL applications due to its appealing properties such as excellent visible transparency, high electron mobility, environmentally friendly nature and ease of fabrication.[10,11] A variety of low-temperature and solution-based methods by using Sol-gel precursors or colloidal nanocrystals to deposit ZnO ETLs have been demonstrated.[10-13]

Despite the successes of applying solution-processed ZnO ETLs in inverted OPVs, a major challenge lies in how to control the intragap states induced by surface defects.[14,15] Low-temperature and solution-processed ZnO ETLs generally have high densities of surface defects such as dangling bonds and surface groups, introducing various intragap energy levels. These intragap states act as recombination centers for photo-generated charge carriers, causing significant photocurrent loss and degrading the charge selectivity of cathode contacts.[15-17] Moreover, surface defects of ZnO thin films are known to be sensitive to adsorption/desorption of oxygen and water molecules at ambient conditions, which may influence the long-term stability of ZnO ETLs and thereby the stability of OPV devices. [18]

A few strategies have been developed to passivate the surface defects of solution-processed ZnO ETLs.[14,16,19-23] For example, employing self-assembled monolayers (SAMs) on top of ZnO films can avoid the direct contact between ETLs and active layers. The introduction of SAMs may result in formation of interfacial dipoles that favor electron extraction.[16,20] However, the defect states in bulk ZnO ETLs cannot be effectively passivated by this

approach. The fabrication of large-area, dense and compact SAMs, which are resistant to subsequent solution-processing procedures, is challenging for future industrial productions. In another strategy, ZnO-polymer composite films are used as ETLs. Coordination polymers such as poly(ethylene oxide) (PEG) and poly(ethylene glycol) (PEO) are used to passivate surface defects of ZnO nanoparticles, leading to improved device performances.[21,22] Nevertheless, there is a tradeoff between effective surface passivation and charge transport properties of the composite films owing to the insulating nature of coordination polymers. A facile and general approach that can effectively passivate the surface defects of low-temperature processed ZnO ETLs is highly desirable and critical to fully exploit their remarkable properties for inverted OPVs.

Here we propose that the surface defects of solution-processed ZnO ETLs can be passivated by specific small molecules. An alkanethiol with bidentate coordination groups, 1,2-ethanedithiol (EDT), is selected to verify this hypothesis. The effects of EDT treatment on the chemical, morphological and electrical properties of thin films based on colloidal ZnO nanocrystals were analyzed. The EDT-treated ZnO nanocrystal films were applied in inverted organic solar cells to investigate the impact of modification of intragap states of the ETLs on device performance. To explore the generality of this passivation approach, the EDT treatment was also applied to ZnO ETLs deposited from Sol-gel precursors.

2. Results and Discussion

2.1 EDT Treatment on ZnO Nanocrystal Films

EDT treatment involves simple procedures of immersing films of ZnO nanocrystals (Figure S1) into a solution containing EDT for 1 min, followed by annealing in a glovebox at 150 ºC for 30 min. For the sake of simplicity, the pristine ZnO nanocrystal thin films are named as P-ZnO films and the EDT-treated ZnO nanocrystal thin films are named as E-ZnO films in the following text. We note that the EDT treatment has previously been demonstrated to be effective in terms of replacing the original long-chain insulating ligands of lead chalcogenide

or cadmium chalcogenide based quantum dots, and the EDT treatment leads to improved inter-particle electronic coupling and enhanced charge transport properties of the quantum dot based films.[24-29]

Fourier transform infrared spectroscopy (FTIR) analyses on the P-ZnO films reveal the presence of hydroxyl groups and carboxylate groups. As shown in Figure 1a, the broad peak at 3390 cm^{-1} corresponds to the hydroxyl groups and the peaks at 1560 and 1420 cm^{-1} correspond to the carboxylate groups. After EDT treatment, the intensities of these absorption peaks are decreased, suggesting that a large fraction of the hydroxyl and carboxylate groups have been removed. Furthermore, the characteristic stretching band of $-CH_2-$ groups at 2920 cm^{-1} becomes evident, implying the binding of EDT molecules onto the surfaces of E-ZnO films.[26,27]

X-ray photoelectron spectroscopy (XPS) analyses reveal surface chemistry of the ZnO nanocrystal films. The survey spectra of the P-ZnO and E-ZnO films are shown in Figure 1b. The most significant change due to EDT treatment is the emergence of the sulfur peaks (inset of Figure 1b). The S 2p peak located at 163.2 eV with a shoulder at 164.3 eV (Figure S2) indicates that EDT molecules were covalently bonded onto the surfaces of ZnO nanocrystals, forming zinc thiolates.[30-32] Figure 1c shows the O 1s core level spectra, which can be de-convoluted into two peaks. The lower-binding-energy peak is associated with the oxygen atoms in a ZnO matrix, *i.e.* O–Zn bonding. The higher-binding-energy peak is attributed to the oxygen-deficient defects, such as oxygen vacancies and hydroxyl O–H groups.[11,33] After EDT treatment, the relative intensity of the higher-binding-energy component significantly decreased, suggesting that the oxygen-deficient defects in the ZnO films are largely removed. These results, together with the FTIR analyses indicate the protonation of thiols to displace the surface groups and passivation of the surface defects. Furthermore, the Zn $2p_{3/2}$ peak shifts towards lower binding energy by 0.2 eV after EDT treatment (Figure 1d). This shift reflects

the higher electron densities around the zinc atoms. The more negative oxidation state of the zinc ions is consistent with the formation of Zn-S bonds, which replaces the original Zn-O bonds of the hydroxyl groups or carboxylate groups.[31] A quantitative depth-profile study on the E-ZnO films was carried out (Figure 1e). With the prolonged sputter time, the atomic ratio of sulfur to zinc is kept in the range of 0.25 to 0.29, indicating that EDT treatment effectively modified all the ZnO nanocrystals in the bulk films which are ~85 nm in thickness.

The surface properties of the ZnO nanocrystal thin films were characterized by contact angle measurements and atomic force microscopy (AFM). As illustrated in Figure S3, the static contact angles of water on the ZnO films increased from 41° to 53° upon the EDT treatment. The fact that the E-ZnO films are more hydrophobic agrees with the EDT treatment induced surfaces with -CH_2-CH_2- groups. AFM measurements show that the E-ZnO and P-ZnO films have comparable root-mean-square (RMS) surface roughness of ~5 nm (Figure S4). The topological images and the corresponding phase images, however, reveal significantly different features. For the P-ZnO films, large domains with sizes of 50-100 nm, due to sintering of small primary particles during the annealing procedure, were observed. In contrast, the E-ZnO films exhibit much smaller domains with sizes of less than 10 nm. We suggest that surface passivation by EDT molecules leads to nanocrystal surfaces with -CH_2-CH_2- groups. Such chemically inert surfaces prevent the growth of the oxide domains at elevated temperatures.

2.2 P3HT:$PC_{61}BM$ Inverted Solar Cells Based on EDT Treated ZnO Nanocrystal Films

The E-ZnO films were applied as ETLs in OPVs with an inverted device structure of ITO/ZnO/poly(3-hexylthiophene) (P3HT): [6-6]-phenyl-C61-butyric acid methyl ester ($PC_{61}BM$)/MoO_x/Ag (Figure 2a). Devices with P-ZnO films as ETLs were also fabricated. The current density-voltage (J-V) and external quantum efficiency (EQE) characteristics of the representative devices are shown in Figure 2b and Figure 2c. The corresponding electrical

output parameters are summarized in Table 1. The results show that upon EDT treatment, the devices exhibit higher PCEs and greater EQE values over the entire photo-responsive spectral range. For the devices with E-ZnO films, an average PCE of 4.8 % was obtained. A champion device exhibited an open circuit voltage (V_{OC}) of 0.61 V, a short current density (J_{SC}) of 11.88 mA/cm^2 and a fill factor (FF) of 0.71, leading to a PCE of 5.1 %. We highlight that, the FF of 0.71 is one of the highest values reported in literature for P3HT:PC_{61}BM-based inverted solar cells, revealing the excellent charge extraction properties of this device. The control devices based on P-ZnO ETLs exhibit a relative low average PCE of 3.8 %. As shown in Figure 2d, the ambient stability of the devices with E-ZnO ETLs is also significantly improved. For unencapsulated P3HT:PC_{61}BM devices, the PCE remained 90 % of the original value after being stored in dark and under ambient conditions for 30 days. In contrast, the PCE of the control device with P-ZnO ETLs degraded to ~60 % of the original value under the same conditions.

To understand the origin of the improved device performance, the P3HT:PC_{61}BM inverted devices were characterized by a number of electrical techniques. First, transient photo-voltage (TPV) measurements indicate that the devices with E-ZnO ETLs exhibit reduced charge recombination rates and enhanced charge extraction characteristics. TPV measurements evaluate the charge carrier decay dynamics under an extraction electric field, providing a direct method to probe the charge populations and charge recombination in a solar cell.[34,35] We carried out TPV measurements under different light intensities, which resulted in V_{OC} ranging from 0.40 to 0.61 V. The carrier lifetime at each V_{OC} was derived from the exponentially fitting of the TPV curves. The capacitance (C) was determined using a procedure of differential charging. The steady-state carrier concentration was obtained by integrating C with respect to the measured V_{OC}.[35] As shown in Figure 3a-3c, the devices with E-ZnO ETLs exhibit longer photogenerated charge carrier lifetimes, smaller capacitance and

reduced steady-state carrier concentrations. Therefore the devices with E-ZnO ETLs show characteristics of reduced charge recombination rates and enhanced charge extraction.[36] Second, dark J-V curves show that EDT treatment significantly improved the selectivity of the cathodes. As shown in Figure 3d, the reverse saturation current for the device with E-ZnO ETL is greatly suppressed compared to the device with P-ZnO ETL while the two devices exhibit similar output current in the forward direction. Third, electron-only devices with a structure of ITO/ZnO/P3HT:$PC_{61}BM$/LiF/Al were fabricated to investigate the electron transport properties of the inverted devices (Figure 3e). An increased current density for the device with E-ZnO ETLs is observed, revealing the improved electron transporting characteristics.[37]

We suggest that for the P3HT:$PC_{61}BM$ devices, other factors, such as optical absorption and morphologies of active layers are not the major reasons for the improved device performance. As shown in AFM images (Figure S5), despite the slightly changed surface-wetting properties of the ZnO films after EDT treatment, the surface roughness and phase profiles of the active layers deposited onto the E-ZnO or P-ZnO films are almost identical. These results suggest that EDT treatment on the ZnO ETLs does not significantly alter the morphologies of the top blend films. Our optical modeling results (Figure S6) show that there are almost no optical-field-dissipation difference for 550 nm and 600 nm illumination of the P3HT:$PC_{61}BM$ active layers in the devices with the P-ZnO films and E-ZnO films, respectively.

2.3 Electronic and Molecule Model of EDT Passivated ZnO Nanocrystal Films

Based on above analyses, we correlate the higher PCE and better stability of the devices with E-ZnO ETLs to the surface-passivation effects. We propose that surface passivation by EDT treatment leads to efficient modulation of the electronic structure and intragap states of the ZnO nanocrystal films. A number of spectroscopic techniques are used to verify this hypothesis. UV-Vis absorption spectra in Figure 4a show an additional broad peak in the

range of 400-600 nm for the E-ZnO films. We attribute this peak to the emergence of an intragap band with high density of states, which is confirmed by the photoluminescence (PL) spectra. As shown in Figure 4b, the PL spectrum (excitation: 310 nm) of the P-ZnO film exhibits a narrow emission peak at ~366 nm corresponding to the band-edge emission and a board peak of visible emission centered at ~545 nm, which is attributed to the defect-related emission.[14,38] After EDT treatment, both the visible emission and the band-edge emission are almost completely quenched. We note that a similar PL quenching phenomenon was observed for the dodecanethiol modified ZnO nanocrystal films.[39] The quenching of PL is consistent with the introduction of a new intragap band that acts as an efficient non-radiative decay channel.

Ultraviolet photoelectron spectroscopy (UPS) measurements provide further information on the band structure of the ZnO films. As shown in Figure 4c, the work function for the P-ZnO and E-ZnO films was determined to be 3.7 and 4.1 eV, respectively. For the P-ZnO films, the position of the valence band edge relative to the Fermi level is 3.6 eV. This fact suggests that the Fermi level is close to the conducting band edge, implying a high electron concentration induced by the defects, such as oxygen vacancies.[40] After EDT treatment, the position of the valence band edge relative to the Fermi level decreases to 2.4 eV. Therefore the Fermi level is moving towards the center of the band gap, suggesting a significant reduction of electron concentration.

Furthermore, the passivation of the surface defects makes the ZnO nanocrystal films less susceptible to oxygen and water molecules in the environment. Figure 4d shows the time-resolved photocurrent decay of the ZnO nanocrystal films in response to pulsed UV illuminations. The photocurrent decay of ZnO films is largely controlled by the adsorption/desorption of water or oxygen molecules.[18] Given that the experiments were

conducted at the same ambient conditions, a slower decay process for the E-ZnO film suggests that the available absorption/desorption sites are decreased.

The above information allows us to conclude that the intragap states of the ZnO nanocrystals were effectively modified by the EDT treatment, introducing a new intragap band (Figure 5a and Figure 5b). In this scenario, the various surface defects including surface groups, such as hydroxyl groups and carboxylate groups, and dangling bonds were passivated by the formation of zinc ethanedithiolates (Figure 5c). The EDT treatment induced intragap band facilitates electron transport in the ETLs while the intragap states induced by the surface defects acts as trapping centers (Figure 5a and Figure 5b). Therefore EDT treatment largely eliminates the recombination centers at the ZnO/active layer interfaces and improves the electron transport properties of the bulk ZnO films. In consequence, EDT treatment suppresses the interfacial bimolecular recombination of the trapped electrons and photogenerated holes, enhances the charge selectivity of the cathode contact and improves the charge extraction properties of the devices. In addition, the E-ZnO films are less susceptible to oxygen and water molecules. This change greatly improves the ambient stability of the ZnO ETLs and thereby the stability of the inverted devices.

Another issue worth discussing is the effect of work-function change caused by the EDT treatment. In general, the work function of the ETLs should match the quasi-Fermi potential of the acceptor material under working conditions. When Fermi-level pinning occurs, the built-in electric field and V_{OC} are largely affected by the difference of the quasi-Fermi levels of the donor and acceptor phases instead of the work-function difference of the charge transport interlayers.[41] According to a report by Fahlman and coworkers, the Fermi-level pinning to the negative polarons of PCBM occurs when the work function of the contacting substrate is lower than 4.3 eV.[42] The work function of both the E-ZnO films and the P-ZnO films is sufficiently low, allowing Fermi-level pinning. Therefore the increase of the work

function of E-ZnO films by 0.4 eV does not degrade the built-in field of the inverted devices.[43]

2.4 TQ1:$PC_{71}BM$ Devices Using E-ZnO Interlayers and Solar Cells based on EDT Passivated Sol-gel Derived ZnO films

We further applied the E-ZnO films to the fabrication of inverted solar cells based on poly[2,3-bis-(3-octyloxyphenyl) quinoxaline-5,8-diyl-alt-thiophene-2,5-diyl] (TQ1): [6,6]-phenyl-C_{71}-butyric acid methyl ester ($PC_{71}BM$) blends. TQ1 is a donor material with deep highest-occupied-molecular-orbit (HOMO) level of 5.7 eV.[44] As shown in Figure 6a and Table 2, the devices with E-ZnO ETLs exhibit an average PCE of 6.0 %. The champion device has a remarkable FF of 0.72 and a PCE of 6.3%, which is the record efficiency for the inverted devices based on the TQ1: fullerene system to date.[21,45-46] In contrast, the average PCE for control devices with P-ZnO films, 5.0%, is much lower. Regarding the device stability, when the devices were either stored in dark or tested upon continuous light illumination, a similar trend that the devices with E-ZnO ETLs are much better than the control devices with P-ZnO ETLs was observed (Figure 6b). Our transfer matrix optical modeling and AFM measurements show that there is also no obvious difference in the absorption and the morphologies of the active layers deposited onto the P-ZnO films and E-ZnO films, respectively (see Figure S7 and Figure S8). Furthermore, electroluminescence (EL) and Fourier-transform photocurrent spectroscopy (FTPS) measurements were used to probe the population of the charge-transfer (CT) states of the TQ1 devices. From the normalized absorption and emission spectra shown in Figure S9, almost identical CT emission and EQE features of the two devices indicate that EDT treatment caused negligible influences on the donor-acceptor interfacial areas.[45] These characterizations indicate that the improved device performance of the TQ1 devices arise from the EDT treatment of the ZnO nanocrystal ETLs. This result leads us to conclude that the E-ZnO films can be applied to improve the

performance of inverted devices based on donor materials with different electronic structures. This feature is different from that of the UV-zone treatment, another widely used technique to passivate the surfaces of solution-processed ZnO.[14,47-48] As reported by So and co-workers, UV-ozone treatment not only passivates the surface defects but also generates excess oxygen at the ZnO surfaces which may oxidize the polymers with higher-lying HOMO energies, such as P3HT, and hence degrade the device performance.[14]

Upon successful attempts of EDT passivation on ZnO nanocrystal films, we further extended the EDT passivation approach to the ZnO films deposited from Sol-gel precursors. Inverted organic solar cells based on Sol-gel derived and EDT treated ZnO films were fabricated using either the P3HT: $PC_{61}BM$ blends or TQ1: $PC_{71}BM$ blends as active layers. Control devices with Sol-gel derived ZnO films without EDT treatment were also fabricated. As shown in Figure 6c and Figure 6d, EDT treatment on the Sol-gel derived ZnO ETLs improves the PCE of the inverted devices, *i.e.* from 3.7% and 4.9% to 4.5% and 6.0% for P3HT:$PC_{61}BM$ and TQ1:$PC_{71}BM$ devices, respectively. The detail device parameters are summarized in Table 2. These results suggest that the EDT modification approach can be a general method to passivate the surface defects of solution-processed ZnO ETLs, thereby improving the performance of the resulting inverted solar cells.

3. Conclusion

In summary, we developed a simple and general method based on EDT treatment to passivate the surface defects and modulate the intragap states of low-temperature solution-processed ZnO films. By using EDT treatment on the P-ZnO films as a model system, we show that the covalently bonding of EDT molecules onto the ZnO surfaces by forming zinc ethanedithiolates efficiently removes various surface defects including surface groups, such as hydroxyl groups and carboxylate groups, and dangling bonds. The chemical changes are accompanied by the modification of intragap states of the ZnO films and the introduction of a

new intragap band, leading to ETLs with enhanced selectivity and better electron transport properties. When the E-ZnO films are applied as ETLs in organic solar cells, the interfacial bimolecular recombination loss is minimized. Furthermore, the well-passivated surfaces of the E-ZnO films are less susceptible to oxygen and water molecules. Therefore the inverted devices with E-ZnO films exhibited higher PCEs and improved ambient stability. We further demonstrated that the facile EDT surface passivation method can be extended to Sol-gel derived ZnO ETLs as well as inverted solar cells with different donor polymers.

Our study provides an excellent example that advances on the surface chemistry, together with new understanding on the electronic properties of interfacial materials are critical for improving the performance of organic solar cells. Considering that solution-processed ZnO films are used as ETLs in many optoelectronic devices, it is of interest to apply the EDT treatment based passivation method to other devices, such as hybrid perovskite solar cells and quantum-dot based solar cells.

4. Experimental Section

Preparation of ZnO Nanocrystal Films and Sol-gel ZnO Films: The colloidal ZnO nanocrystals were synthesized by controlled hydrolysis of zinc acetate in an alcoholic basic solution and dissolved in a mixed solvent of chloroform and methanol (3:1 by volume) as published else where. [18,49] Patterned ITO substrates were ultrasonic cleaned with acetone, ethanol and deionized water, respectively, and then were treated in UV-ozone for 15min. The ZnO nanocrystal solution with a concentration ~15 mg/ml was spin-cast at 4000 rpm to form P-ZnO films with thickness of ~85 nm after annealling at 150 ºC for 30 min in a nitrogen-filled glove box. The ZnO precursor solution was prepared by dissolving 15 mg/mL of $Zn(acac)_2$ hydrate in absolute ethanol. The solution was stirred for 3 h at 50 ºC and subsequently filtered through a PTFE filter (0.22 μm). Sol-gel ZnO films were obtained by spin-coating of the precursor solution at 2000 rpm, followed by annealing at 130 ºC for 1 min.

EDT Passivation of ZnO Films: Regarding the EDT treatment, the P-ZnO films were soaked

in an acetonitrile solution containing EDT (0.1% by volume) for 1 min. Then the films were annealed at 150 ºC for 30 min in a nitrogen-filled glove box to obtain E-ZnO films. For Sol-gel ZnO films, a same EDT-soaking procedure was carried out and the EDT-soaked films were further annealed at 130 ºC for 10 min in glove box.

ZnO Thin Films Characterization: The FTIR spectra of ZnO nanocrystals films with and without EDT treatment were recorded on a Bruker Tensor 27 spectrophotometer. XPS and UPS spectra were collected on a Thermo ESCALAB 250 equipment in an ultra high vacuum chamber with a vacuum $<10^{-10}$ Torr. He I (21.22 eV) radiation line from a discharge lamp, with an experimental resolution of 0.1 eV, was used in the UPS measurements. AFM images were obtained using a Veeco Multi Mode V atomic force microscopy. Contact angle measurements were carried out using a CAM 200 optical contact angle meter. UV-Vis absorption spectra were obtained using a Shimadzu UV-3600 spectrometer. Steady-state PL measurements were acquired using an Edinburgh Instruments FLS920 fluorescence spectrometer. A spectroscopic ellipsometer (J.A.Woollam M-2000) was used to determine the optical constants and thicknesses of the ZnO films and active layers of the solar cells.

UV Phototconduction Characterization: The UV photoconductive behaviors of the P-ZnO and E-ZnO films were evaluated by using a planar device configuration.[1] A 150-nm-thick Al electrode was evaporated through a shadow mask to form "T"-shape contacts on the ZnO films deposited onto pre-cleaned glass substrates. The spacing between the electrodes was 200 μ m and the length was 3 mm. UV excitation was provided by a UV light-emitting diode (370 nm) and focused onto the devices with a spot size of *ca.* 2 mm.

Fabrication and Characterization of Inverted Organic Solar Cells: For the P3HT: $PC_{61}BM$ solar cells, a solution of P3HT (Rieke Metals, #4002-E) and $PC_{61}BM$ purchased from Solenne (1:0.8 by weight, 15 mg/ml) in 1, 2-dichlorobenzene was prepared by stirring for 12 h at 50 ºC in a glove box. The blend solution was deposited onto the ZnO thin films by spin-coating

at 700 rpm for 18 s, followed by a slow solvent-evaporation process. The resulting active layer, ca. 200 nm in thickness, was annealed at 110 ºC for 12 min in a glove box. Inverted organic solar cells based on TQ1 donors were fabricated by spin-coating a solution of TQ1:$PC_{71}BM$ (9:27 mg/mL) in 1,2-dichlorobenzene at 650 rpm for 60 s and then at 3000 rpm for 30 s. Bi-layer top electrodes of MoO_x/Ag (7/100 nm) were deposited by thermal evaporation under a base pressure of 6×10^{-7} Torr (Kurt J. Lesker Mini Spectra). The device area defined by the overlapping area (square) of the ITO and Ag electrodes was 7.25 mm^2. J-V characterization of the solar cells were performed with a Keithley 2400 source meter controlled by a LabVIEW program under simulated air mass (AM) 1.5 G irradiation at 100 mW cm^{-2} using a Xe lamp-based solar simulator (Newport 91160). EQE measurements were performed in air based on a home made setup consisting of a Keithley 2400 Source Measure Unit and Newport monochromator.The light intensity was calibrated using a Newport standard silicon cell 91150 and corrected for spectral mismatch.

Transient Photovoltage, Electroluminescence and Fourier-Transform Photocurrent Spectroscopy: For the TPV measurements, the solar cells were connected to a digital oscilloscope (Tektronix TDS 3012C) with an input impedance of 1 MΩ. The intensity of white light was referred here as a "light bias". The light was used to control the V_{OC} of the devices. A laser with a wavelength of 532 nm was used as the optical perturbation. The pulse duration was set to 1 ms and the frequency to 100 Hz. The frequency, light intensity, and pulse duration were constant, while the photocurrent transient was measured at an impedance of 50 Ω. FTPS spectra were measured on a Vertex 70 from Bruker optics. EL spectra were obtained with a Shamrock sr 303i spectrograph from Andor Tech., coupled to a Newton EM-CCD Si array detector.

Supporting Information

Supporting Information is available from the Wiley Online Library or from the author.

Acknowledgements

This work is financially supported by the National High Technology Research and Development Program of China (2011AA050520), the National Basic Research Program of China (973 Program, 2012CB932402), the National Natural Science Foundation of China (51172203), Natural Science Funds for Distinguished Young Scholar of Zhejiang Province (R4110189) and the Public Welfare Project of Zhejiang Province (2013C31057). Financial supports from Swedish Energy Agency (Energimyndigheten) and the Swedish Research Council (VR) are also greatly appreciated. F.G. acknowledges the financial support of the European Commission under a Marie Curie Intra-European Fellowship for Career Development. The authors are grateful to Clemens Veit and Martin Sessler for device fabrication and insightful discussions. Dr. Ergang Wang at Chalmers University of Technology for TQ1 materials and Prof. Olle Inganäs at Linköping University for Lab facilities are also greatly appreciated.

Received: ((will be filled in by the editorial staff))
Revised: ((will be filled in by the editorial staff))
Published online: ((will be filled in by the editorial staff))

[1] G. Yu, J. Gao, J. C. Hummelen, F. Wudl, A. J. Heeger, *Science* **1995**, 270, 1789-1791.

[2] J. J. M. Halls, C. A. Walsh, N. C. Greenham, E. A. Marseglia, R. H. Friend, S. C. Moratti, A. B. Holmes, *Nature* **1995**, 376, 498-500.

[3] G. Li, V. Shrotriya, J. Huang, Y. Yao, T. Moriarty, K. Emery, Y. Yang, *Nat. Mater.* **2005**, 4, 864-868.

[4] J. You, L. Dou, K. Yoshimura, T. Kato, K. Ohya, T. Moriarty, K. Emery, C.-C. Chen, J. Gao, G. Li, Y. Yang, *Nat. Commun.* **2013**, 4, 1446.

[5] F. C. Krebs, S. A. Gevorgyan, J. Alstrup, *J. Mater. Chem.* **2009**, 19, 5442-5451.

[6] M. Jorgensen, K. Norrman, S. A. Gevorgyan, T. Tromholt, B. Andreasen, F. C. Krebs, *Adv. Mater.* **2012**, 24, 580-612.

[7] T. Yang, M. Wang, C. Duan, X. Hu, L. Huang, J. Peng, F. Huang, X. Gong, *Energy Environ. Sci.* **2012**, 5, 8208-8214.

[8] Y. Zhou, F. Li, S. Barrau, W. Tian, O. Inganäs, F. Zhang, *Sol. Energy Mater. Sol. Cells* **2009**, 93, 497-500.

[9] C. E. Small, S. Chen, J. Subbiah, C. M. Amb, S.-W. Tsang, T.-H. Lai, J. R. Reynolds, F. So, *Nat. Photon.* **2012**, 6, 115-120.

[10] S. Bai, Z. Wu, X. Xu, Y. Jin, B. Sun, X. Guo, S. He, X. Wang, Z. Ye, H. Wei, X. Han, W. Ma, *Appl. Phys. Lett.* **2012**, 100, 203906.

[11] Y. Sun, J. H. Seo, C. J. Takacs, J. Seifter, A. J. Heeger, *Adv. Mater.* **2011**, 23, 1679-1683.

[12] J. You, C.-C. Chen, L. Dou, S. Murase, H.-S. Duan, S. A. Hawks, T. Xu, H. J. Son, L. Yu, G. Li, Y. Yang, *Adv. Mater.* **2012**, 24, 5267-5272.

[13] P. de Bruyn, D. J. D. Moet, P. W. M. Blom, *Org. Electron.* **2010**, 11, 1419-1422.

[14] S. Chen, C. E. Small, C. M. Amb, J. Subbiah, T.-h. Lai, S.-W. Tsang, J. R. Manders, J. R. Reynolds, F. So, *Adv. Energy. Mater.* **2012**, 2, 1333-1337.

[15] M. Hartel, S. Chen, B. Swerdlow, H.-Y. Hsu, J. Manders, K. Schanze, F. So, *ACS Appl.*

Mater. Interfaces **2013**, 5, 7215-7218.

[16] S. K. Hau, H.-L. Yip, H. Ma, A. K.-Y. Jen, *Appl. Phys. Lett.* **2008**, 93, 233304.

[17] A. Gadisa, Y. Liu, E. T. Samulski, R. Lopez, *Appl. Phys. Lett.* **2012**, 100, 253903.

[18] Y. Jin, J. Wang, B. Sun, J. C. Blakesley, N. C. Greenham, *Nano Lett.* **2008**, 8, 1649-1653.

[19] Y. E. Ha, M. Y. Jo, J. Park, Y.-C. Kang, S.-J. Moon, J. H. Kim, *Synth. Met.* **2014**, 187, 113-117.

[20] Y. E. Ha, M. Y. Jo, J. Park, Y.-C. Kang, S. I. Yoo, J. H. Kim, *J. Phys. Chem. C* **2013**, 117, 2646-2652.

[21] S. Shao, K. Zheng, T. Pullerits, F. Zhang, *ACS Appl. Mater. Interfaces* **2012**, 5, 380-385.

[22] S. B. Jo, J. H. Lee, M. Sim, M. Kim, J. H. Park, Y. S. Choi, Y. Kim, S.-G. Ihn, K. Cho, *Adv. Energy. Mater.* **2011**, 1, 690-698.

[23] S.-H. Liao, H.-J. Jhuo, Y.-S. Cheng, S.-A. Chen, *Adv. Mater.* **2013**, 25, 4766-4771.

[24] R. Zhou, R. Stalder, D. Xie, W. Cao, Y. Zheng, Y. Yang, M. Plaisant, P. H. Holloway, K. S. Schanze, J. R. Reynolds, J. Xue, *ACS Nano* **2013**, 7, 4846-4854.

[25] G. Konstantatos, L. Levina, A. Fischer, E. H. Sargent, *Nano Lett.* **2008**, 8, 1446-1450.

[26] J. M. Luther, M. Law, Q. Song, C. L. Perkins, M. C. Beard, A. J. Nozik, *ACS Nano* **2008**, 2, 271-280.

[27] J. Tang, L. Brzozowski, D. A. R. Barkhouse, X. Wang, R. Debnath, R. Wolowiec, E. Palmiano, L. Levina, A. G. Pattantyus-Abraham, D. Jamakosmanovic, E. H. Sargent, *ACS Nano* **2010**, 4, 869-878.

[28] Y. Liu, M. Gibbs, J. Puthussery, S. Gaik, R. Ihly, H. W. Hillhouse, M. Law, *Nano Lett.* **2010**, 10, 1960-1969.

[29] D. A. R. Barkhouse, A. G. Pattantyus-Abraham, L. Levina, E. H. Sargent, *ACS Nano* **2008**, 2, 2356-2362.

[30] S.-Z. Deng, H.-M. Fan, M. Wang, M.-R. Zheng, J.-B. Yi, R.-Q. Wu, H.-R. Tan, C.-H.

Sow, J. Ding, Y.-P. Feng, K.-P. Loh, *ACS Nano* **2009**, 4, 495-505.

[31] J. Singh, J. Im, J. E. Whitten, J. W. Soares, D. M. Steeves, *Langmuir* **2009**, 25, 9947-9953.

[32] J. Dvorak, T. Jirsak, J. A. Rodriguez, *Surf. Sci.* **2001**, 479, 155-168.

[33] X. Q. Wei, B. Y. Man, M. Liu, C. S. Xue, H. Z. Zhuang, C. Yang, *Physica B.* **2007**, 388, 145-152.

[34] P. P. Boix, J. Ajuria, R. Pacios, G. Garcia-Belmonte, *J. Appl. Phys.* **2011**, 109, 074514.

[35] C. G. Shuttle, B. O'Regan, A. M. Ballantyne, J. Nelson, D. D. C. Bradley, J. de Mello, J. R. Durrant, *Appl. Phys. Lett.* **2008**, 92, 093311.

[36] G. Garcia-Belmonte, P. P. Boix, J. Bisquert, M. Sessolo, H. J. Bolink, *Sol. Energy Mater. Sol. Cells* **2010**, 94, 366-375.

[37] S. Liu, K. Zhang, J. Lu, J. Zhang, H.-L. Yip, F. Huang, Y. Cao, *J. Am. Chem. Soc.* **2013**, 135, 15326-15329.

[38] V. Ischenko, S. Polarz, D. Grote, V. Stavarache, K. Fink, M. Driess, *Adv. Funct. Mater.* **2005**, 15, 1945-1954.

[39] M. A. Garcia, J. M. Merino, E. Fernández Pinel, A. Quesada, J. de la Venta, M. L. Ruíz González, G. R. Castro, P. Crespo, J. Llopis, J. M. González-Calbet, A. Hernando, *Nano Lett.* **2007**, 7, 1489-1494.

[40] B. Ehrler, K. P. Musselman, M. L. Böhm, F. S. F. Morgenstern, Y. Vaynzof, B. J. Walker, J. L. MacManus-Driscoll, N. C. Greenham, *ACS Nano* **2013**, 7, 4210-4220.

[41] E. L. Ratcliff, B. Zacher, N. R. Armstrong, *J. Phys. Chem. Lett.* **2011**, 2, 1337-1350.

[42] Q. Bao, X. Liu, S. Braun, M. Fahlman, *Adv. Energy. Mater.* **2013**, DOI:10.1002/aenm.201301272.

[43] J. Reinhardt, M. Grein, C. Bühler, M. Schubert, U. Würfel, *Adv. Energy. Mater.* **2014**, DOI:10.1002/aenm.201400081.

[44] E. Wang, L. Hou, Z. Wang, S. Hellström, F. Zhang, O. Inganäs, M. R. Andersson, *Adv. Mater.* **2010**, 22, 5240-5244.

[45] Z. Tang, L. M. Andersson, Z. George, K. Vandewal, K. Tvingstedt, P. Heriksson, R. Kroon, M. R. Andersson, O. Inganäs, *Adv. Mater.* **2012**, 24, 554-558.

[46]Z. Ma, Z. Tang, E. Wang, M. R. Andersson, O. Inganäs, F. Zhang, *J. Phys. Chem. C* **2012**, 116, 24462-24468.

[47] J. M. Cho, S.-W. Kwak, H. Aqoma, J. W. Kim, W. S. Shin, S.-J. Moon, S.-Y. Jang, J. Jo, *Org. Electron.* **2014**, 15, 1942-1950.

[48] P. Adhikary, S. Venkatesan, N. Adhikari, P. P. Maharjan, O. Adebanjo, J. Chen, Q. Qiao, *Nanoscale* **2013**, 5, 10007-10013.

[49] B. Sun, H. Sirringhaus, *Nano Lett.* **2005**, 5, 2408-2413.

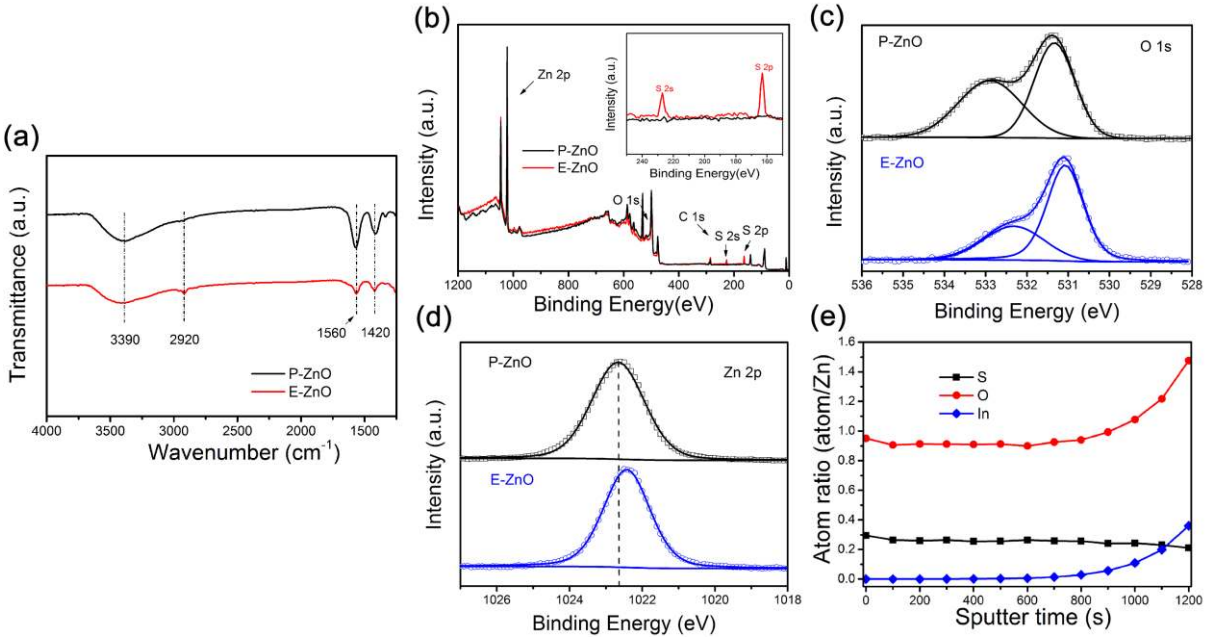

Figure 1. a) FTIR spectra of a P-ZnO film (black curve) and the corresponding E-ZnO film (red curve) on a CaF_2 substrate. b) XPS survey spectra of a P-ZnO film and an E-ZnO film. The inset is the enlarged S spectra showing the occurrence of S peaks after EDT treatment. c) O1s and (d) Zn 2p spectra of the P-ZnO film (square) and the E-ZnO film (circle). e) Depth profiles of the atom ratios of S/Zn, O/Zn and In/Zn in E-ZnO film.

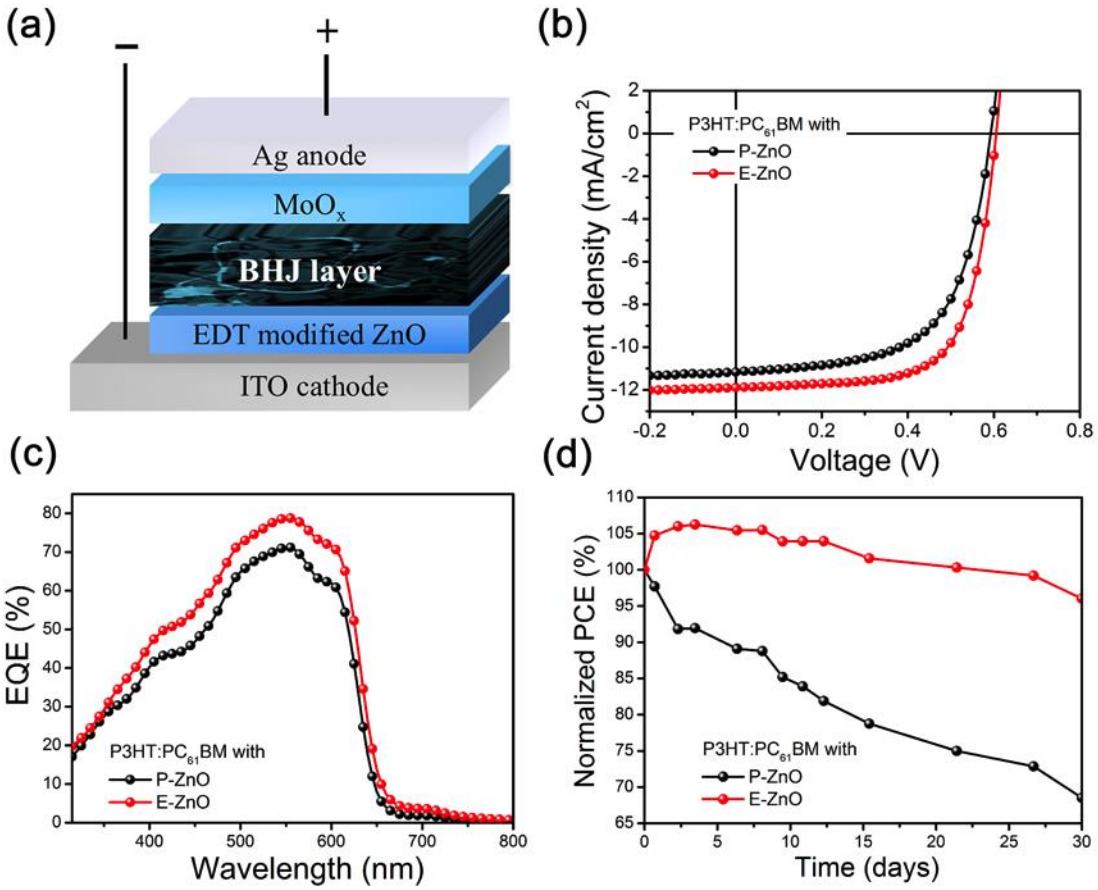

Figure 2. Inverted devices based on P3HT:PC_{61}BM blends. a) Schematic device structure. (b) Light J-V characteristics and c) EQE curves of the devices using E-ZnO films or P-ZnO films as ETLs, respectively. d) Normalized PCE as a function of storage time (dark and ambient conditions) for devices using E-ZnO films or P-ZnO films as ETLs, respectively.

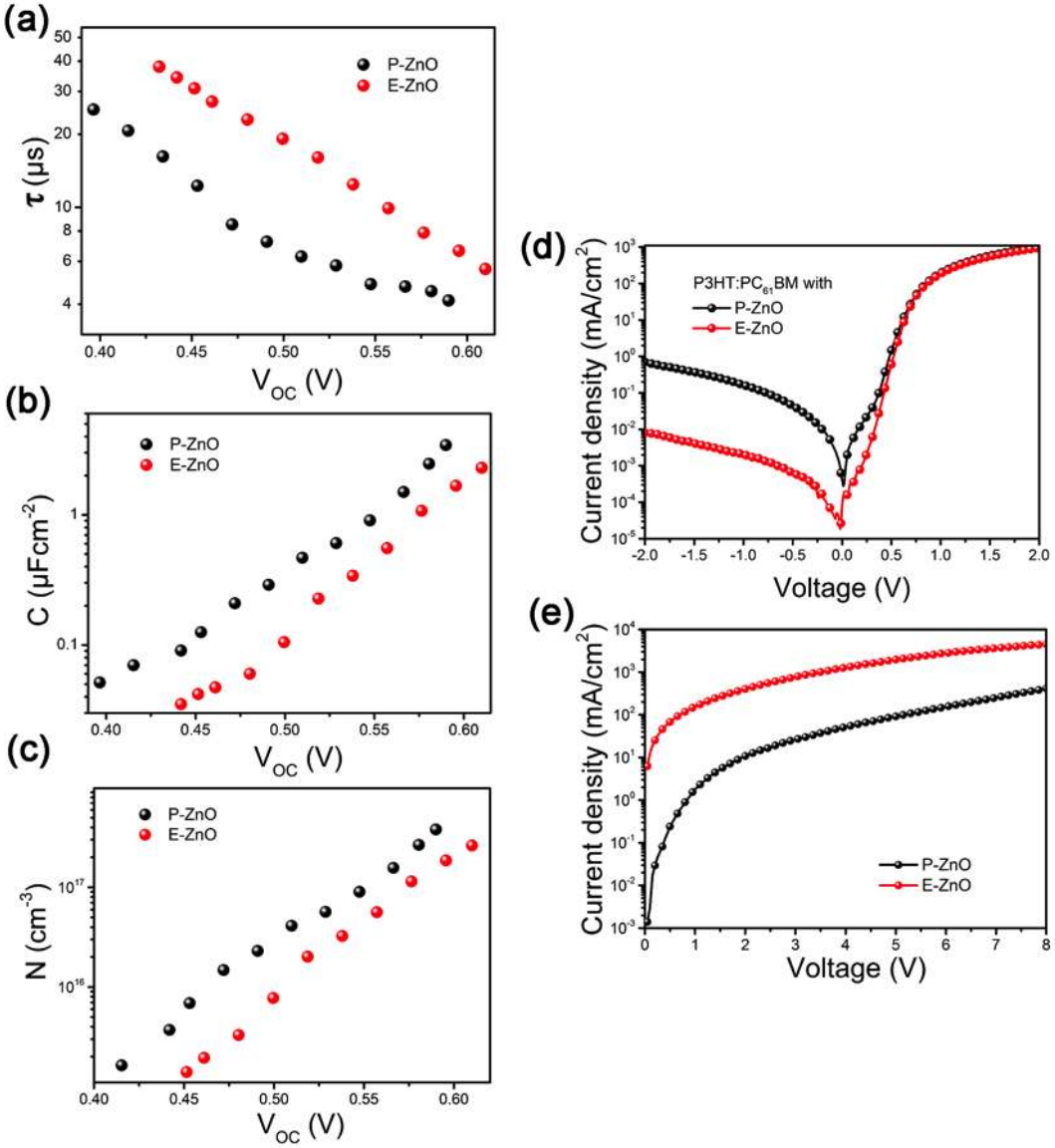

Figure 3. Analyses on the devices with E-ZnO films or P-ZnO films. a)-c) Charge carrier life time, differential capacitance and steady-state carrier concentration vs V_{OC} for inverted P3HT:PC_{61}BM devices with P-ZnO films (black) or E-ZnO films (red) as electron transport interlayers, respectively. d) Dark J-V measurements of the inverted P3HT:PC_{61}BM devices with P-ZnO films (black) or E-ZnO films (red) as electron transport interlayers, respectively. e) J-V curves of electron-only devices (ITO/ZnO/P3HT:PC_{61}BM/LiF/Al) with E-ZnO films or P-ZnO films, respectively.

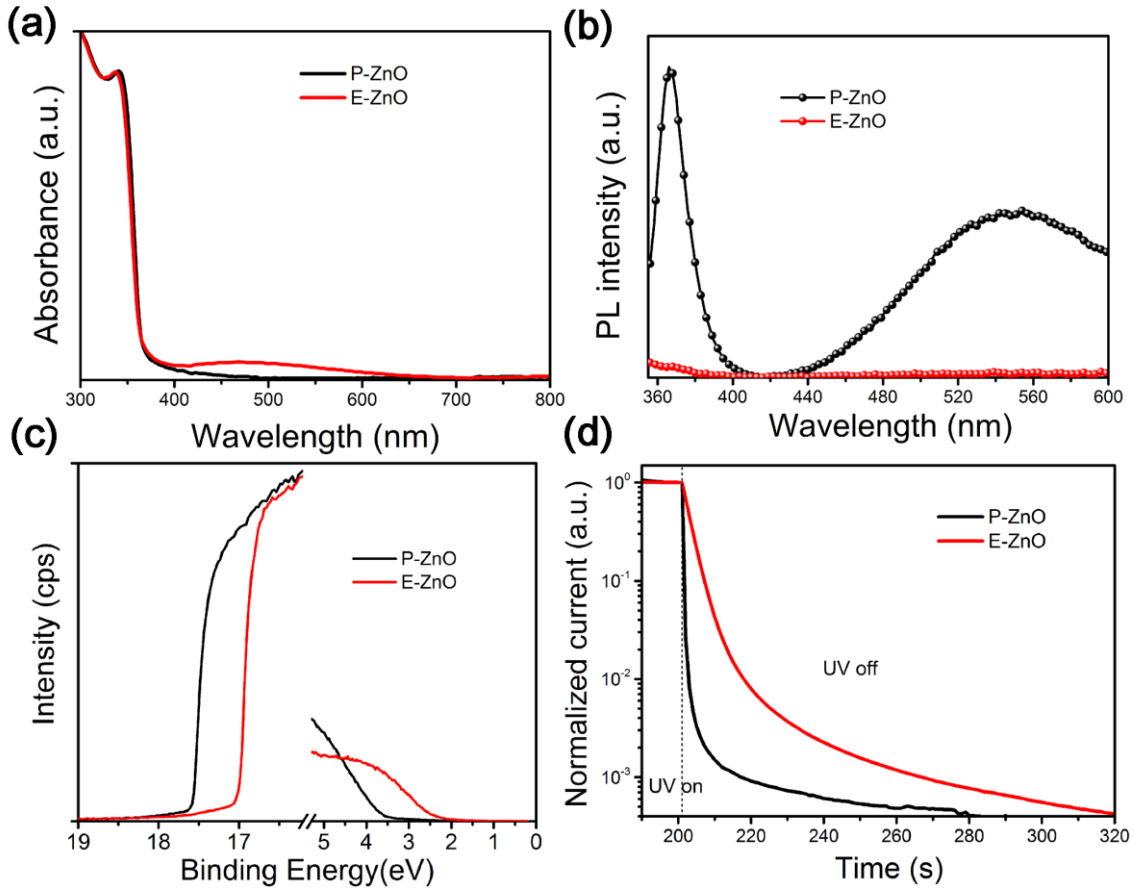

Figure 4. Electronic and electrical properties of the E-ZnO films and the P-ZnO films. a) Normalized UV-Vis absorption spectra, b) steady-state PL spectra excited at 310 nm, c) UPS spectra and d) Normalized time-resolved photocurrent decay characteristics.

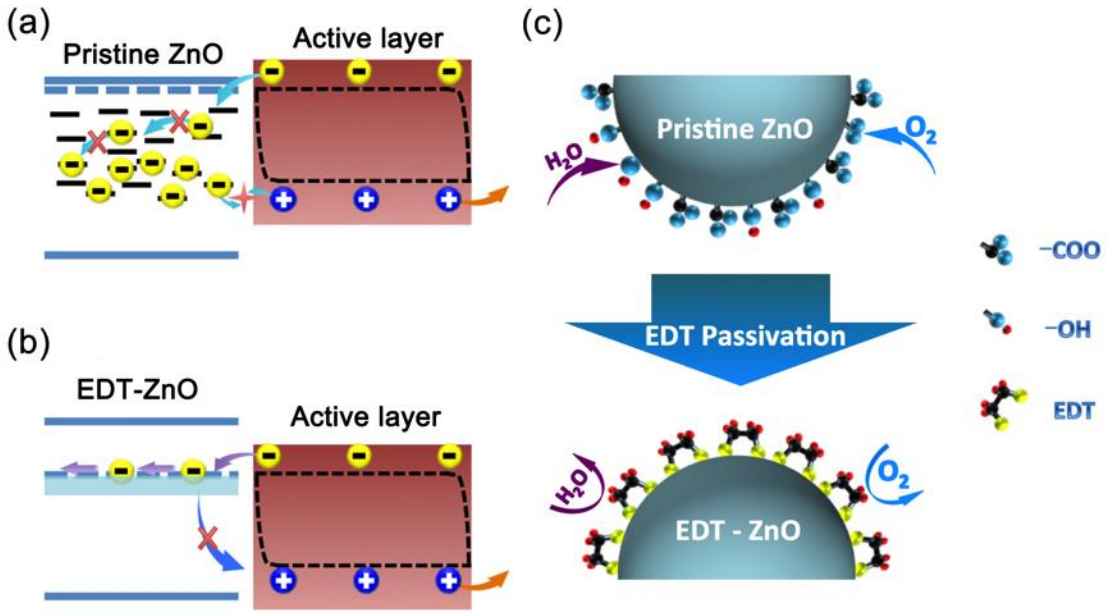

Figure 5. The impact of EDT treatment on the ZnO films and devices with films of ZnO nanocrystals as ETLs. a) The pristine ZnO films have various intragap states which act as recombination centers for photogenerated charges. b) After EDT treatment, the various intragap states due to surface defects are modified to a new intragap band. This new intragap band facilitates electron transport in the ETLs, thereby suppressing the interfacial bimolecular recombination and enhancing the charge extraction properties of the devices. c) Schematic representations showing that the various surface groups are removed and EDT molecules are covalently bound onto the ZnO surface. The excellent surface passivation makes the ZnO films less susceptible to oxygen and water molecules.

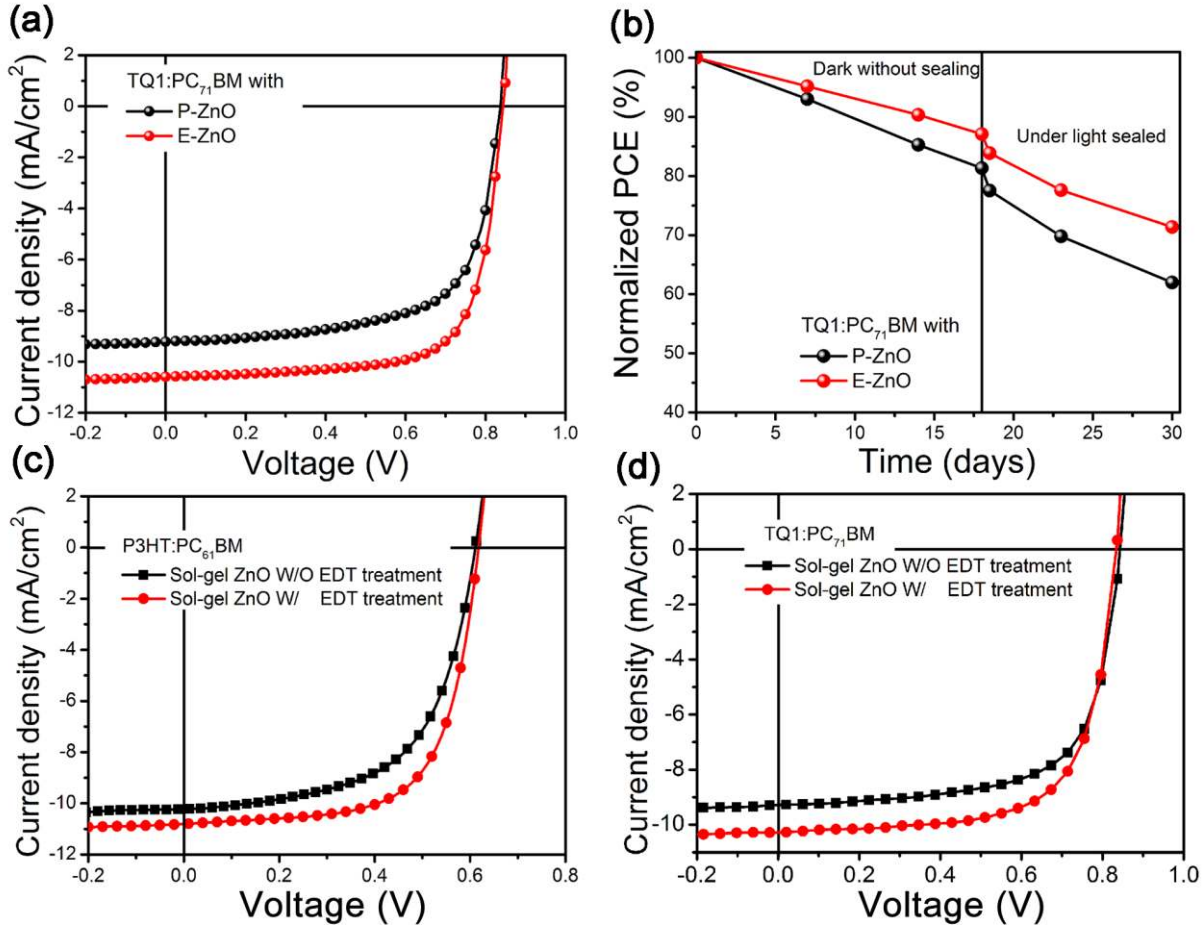

Figure 6. a) J-V characteristics of inverted TQ1:$PC_{71}BM$ devices with E-ZnO films or P-ZnO films as ETLs, respectively. b) Normalized PCEs as a function of storage time of TQ1 based devices. The devices were stored in dark under ambient conditions (1-18 days) followed by encapsulation and then continuous illumination under 100 mW cm^{-2} AM 1.5 solar simulator conditions. c) Light J-V characteristics of inverted P3HT:$PC_{61}BM$ devices and inverted TQ1:$PC_{71}BM$ solar cells (d) based on Sol-gel ZnO ETLs with and without EDT passivation.

Table 1. Device parameters of the inverted P3HT:$PC_{61}BM$ solar cells with E-ZnO films or P-ZnO films as ETLs.

ETLs	V_{OC} (V)	J_{SC} (mA cm^{-2})	FF	Best PCE (%)	Average PCE (%)
P-ZnO film	0.59	11.24	0.63	4.1	3.8 ±0.3
E-ZnO film	0.61	11.88	0.71	5.1	4.8 ±0.3

Table 2. Summary of device parameters of the inverted TQ1:$PC_{71}BM$ devices with E-ZnO films or P-ZnO films as ETLs and inverted organic solar cells based on ZnO films deposited from Sol-gel precursors.

Device configuration	V_{OC} (V)	J_{SC} (mA cm^{-2})	FF	Best PCE (%)	Average PCE (%)
P-ZnO/ TQ1:$PC_{71}BM$	0.84	9.45	0.67	5.3	5.0 ±0.3
E-ZnO/ TQ1:$PC_{71}BM$	0.85	10.42	0.72	6.3	6.0 ±0.3
Sol-gel ZnO/P3HT:$PC_{61}BM$	0.61	10.23	0.59	3.7	3.3 ± 0.4
Sol-gel ZnO-EDT/P3HT:$PC_{61}BM$	0.61	10.98	0.67	4.5	4.1 ± 0.4
Sol-gel ZnO/TQ1:$PC_{71}BM$	0.83	9.15	0.65	4.9	4.5 ± 0.4
Sol-gel ZnO-EDT/TQ1:$PC_{71}BM$	0.83	10.35	0.69	6.0	5.6 ± 0.4

The table of contents entry: A general and efficient molecular passivation strategy of solution-processed ZnO thin films using ethanedithiol (EDT) is developed to modify the defect and intragap states of the electron transporting interlayers in inverted organic solar cells. The efficiency and long-term air stability of devices based on EDT passivated ZnO interlayers were significant improved.

Keyword: organic solar cells, ZnO thin film, electron transporting interlayers, intragap states, molecular passivation

Sai Bai, Yizheng Jin, Xiaoyong Liang, Zhizhen Ye, Zhongwei Wu, Baoquan Sun,* Zaifei Ma, Zheng Tang, Jianpu Wang, Uli Würfel, Feng Gao,* and Fengling Zhang*

Ethanedithiol Treatment on Solution-Processed ZnO Thin Films: Controlling The Intragap States of Electron Transporting Interlayers for Efficient and Stable Inverted Organic Photovoltaics

ToC figure:

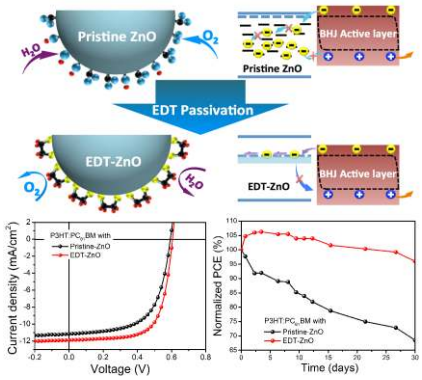

Submitted to ADVANCED ENERGY MATERIALS

Supporting Information

for *Adv. Energy Mater.*, DOI: 10.1002/aenm.((please add manuscript number))

Ethanedithiol Treatment on Solution-Processed ZnO Thin Films: Controlling The Intragap States of Electron Transporting Interlayers for Efficient and Stable Inverted Organic Photovoltaics

Sai Bai,[1] Yizheng Jin,[1] Xiaoyong Liang,[1] Zhizhen Ye,[1] Zhongwei Wu,[2] Baoquan Sun,[2*] Zaifei Ma,[3] Zheng Tang,[3] Jianpu Wang,[4] Uli Würfel,[5,6] Feng Gao,[3*] and Fengling Zhang [3]*

Dr. S. Bai, Dr. Y. Jin, X. Liang, Prof. Z.Ye,
[1] State Key Laboratory of Silicon Materials, Department of Materials Science and Engineering, Cyrus Tang Center for Sensor Materials and Application, and Center for Chemistry of High-Performance and Novel Materials, Zhejiang University, Hangzhou 310027, China
E-mail: yizhengjin@zju.edu.cn
Z. Wu, Prof. B. Sun
[2] Jiangsu Key Laboratory for Carbon-Based Functional Materials & Devices, Institute of Functional Nano & Soft Materials (FUNSOM), Soochow University,
199 Ren'ai Road, Suzhou 215123, China
E-mail:bqsun@suda.edu.cn
Dr. Z. Ma, Dr. Z. Tang, Dr. F. Gao, Dr. F. Zhang3
[3] Department of Physics, Chemistry and Biology (IFM), Linköping University, SE-581 83 Linköping, Sweden
E-mail:fengga@ifm.liu.se
Prof. J. Wang
[4] Institute of Advanced Materials, Nanjing Tech University, Nanjing 210009, China
Dr. U. Würfel
[5] Fraunhofer Institute for Solar Energy Systems ISE, Heidenhofstr. 2, 79110 Freiburg, Germany
Dr. U. Würfel
[6] Materials Research Centre FMF, University of Freiburg,
Stefan-Meier-Str. 21, 79104 Freiburg, Germany

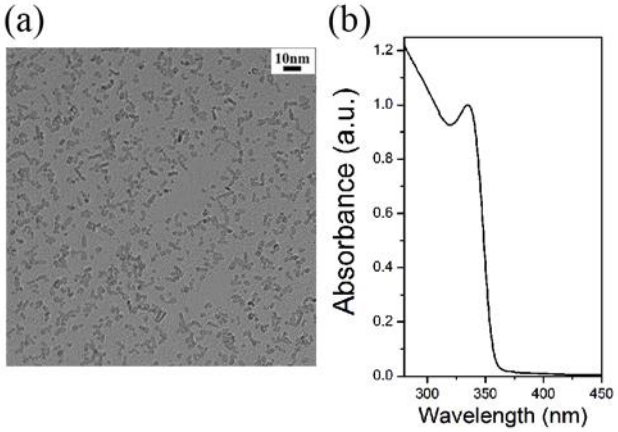

Figure S1. ZnO nanocrystals. a) Transmission electron microscopy (TEM) image and b) UV-vis absorption spectrum of a solution of colloidal ZnO nanocrystals.

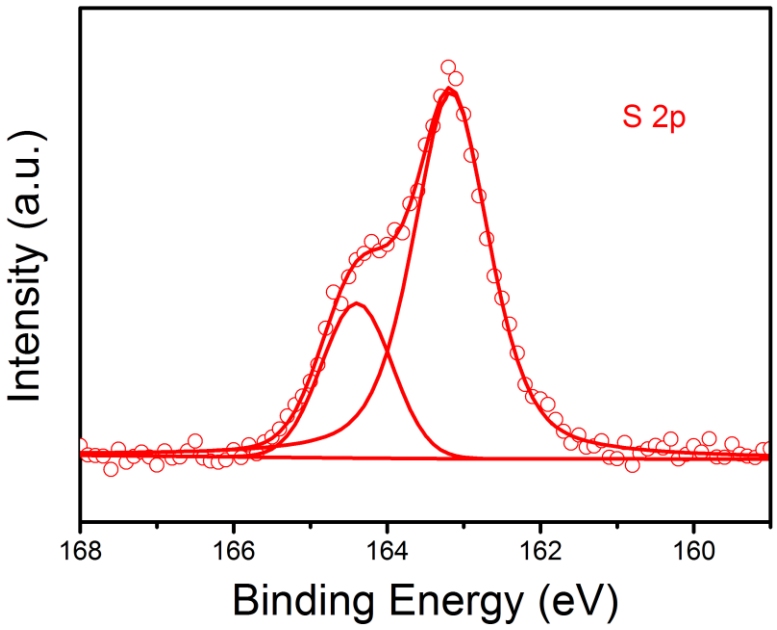

Figure S2. S 2p XPS spectrum of the E-ZnO film.

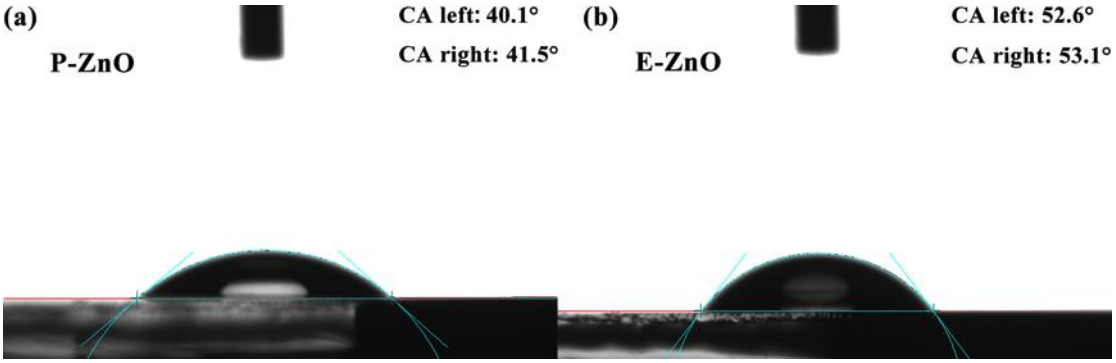

Figure S3. Images showing the contact angles of water on the P-ZnO film (a) and the E-ZnO film (b), respectively.

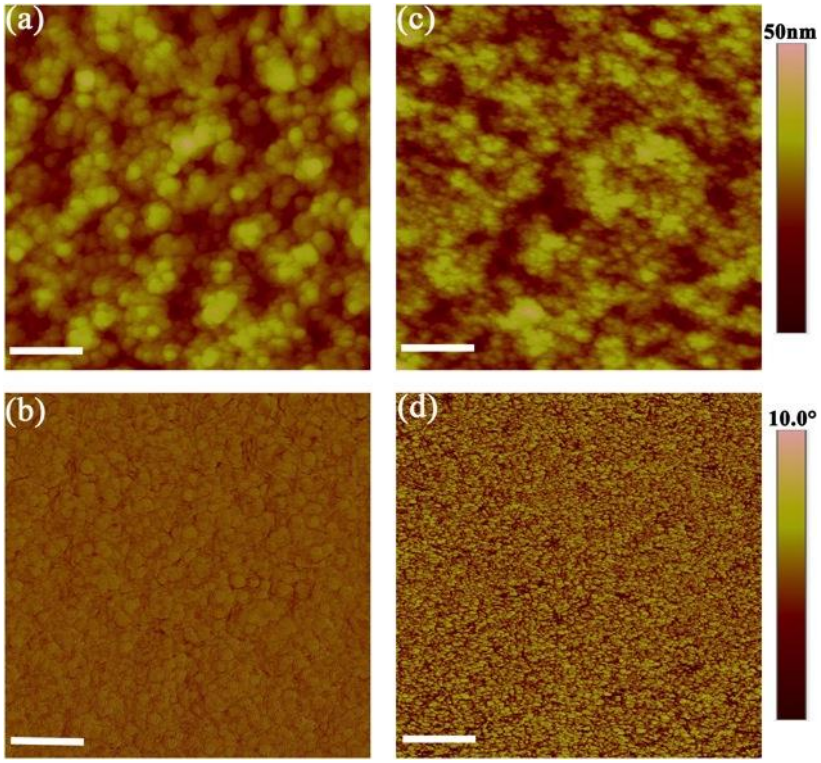

Figure S4. AFM characterizations. a) AFM topography and the corresponding phase image (b) of the P-ZnO films. c) AFM topography and the corresponding phase image (d) of the E-ZnO films. The scan area for both images is 2 μm × 2 μm. Scale bar: 400 nm.

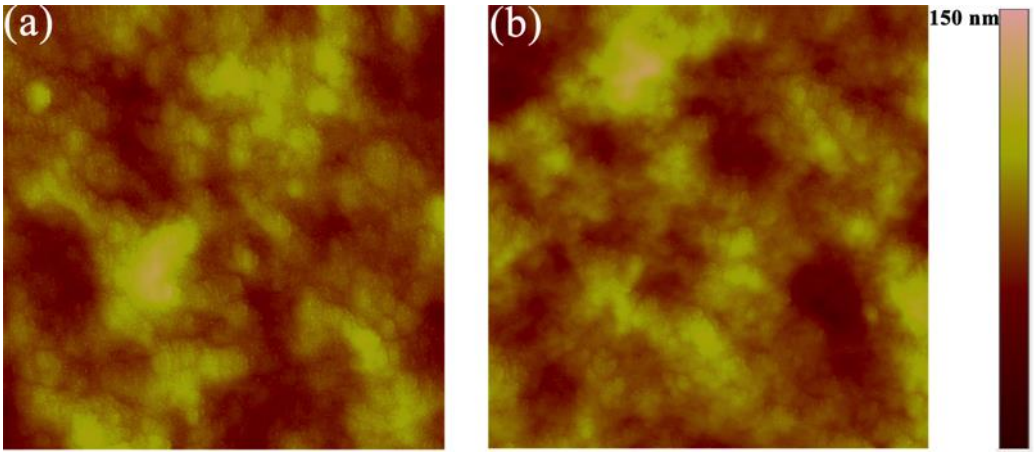

Figure S5. AFM (5×5 μm) topography images of P3HT:$PC_{61}BM$ blends deposited onto (a) the P-ZnO film and (b) the E-ZnO film, respectively.

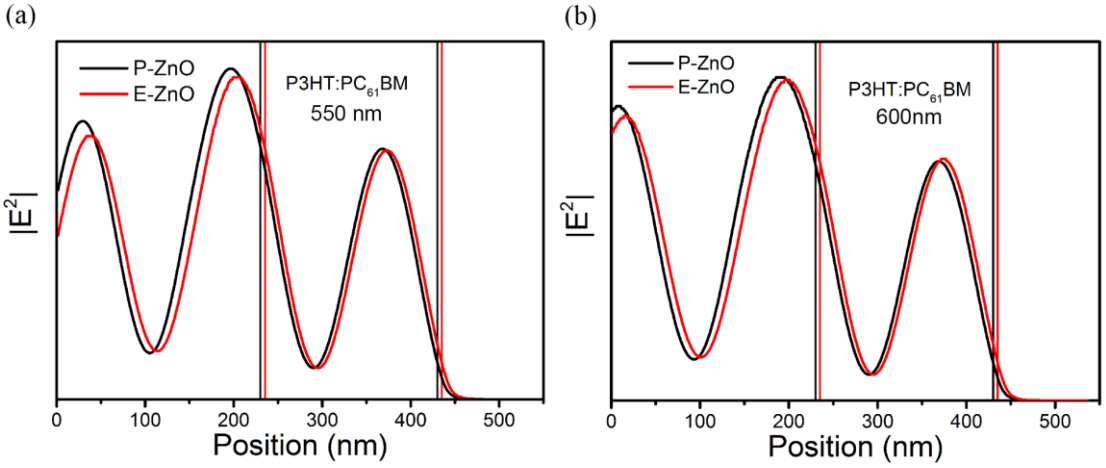

Figure S6. Optical field plot of 550 nm (a) and 600 nm (b) irradiation for a 200 nm P3HT:$PC_{61}BM$ layer for devices based on P-ZnO and E-ZnO interlayers. The transfer matrix approach was used to model the optical electric field distribution the active layer.[1] The optical constants for ITO, MoO_x and Ag are taken from the literatures. [2-4]

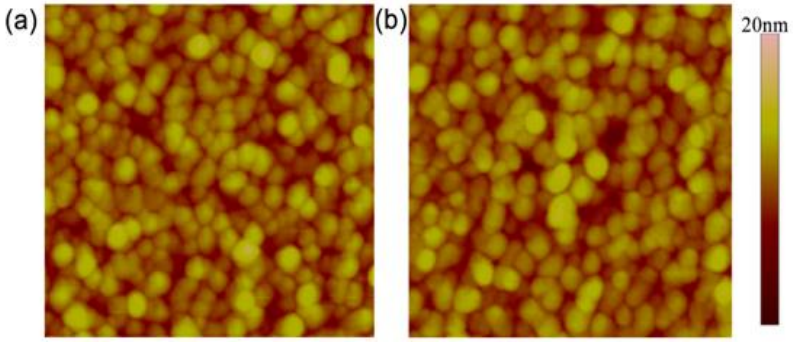

Figure S7. AFM (2×2 μm) topography images of TQ1:$PC_{71}BM$ blends deposited onto (a) the P-ZnO film and (b) the E-ZnO film, respectively.

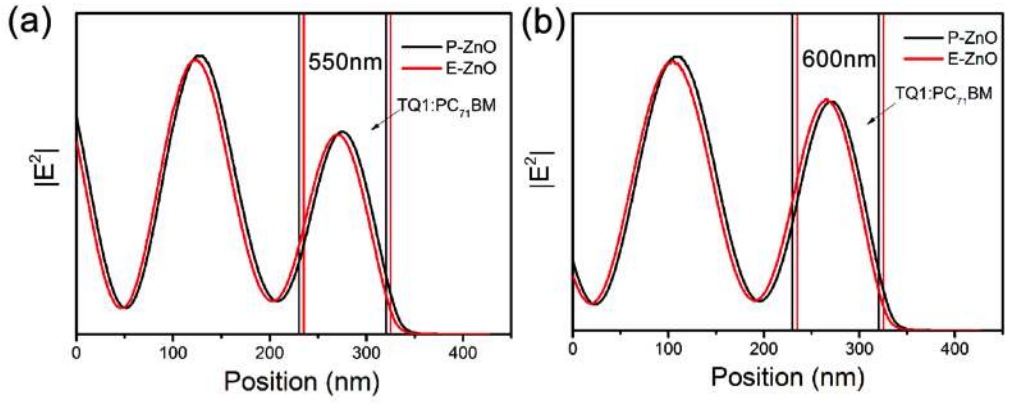

Figure S8. Optical field plot of 550 nm (a) and 600 nm (b) irradiation for a 90 nm TQ1:$PC_{71}BM$ layer for devices based on P-ZnO and E-ZnO interlayers, respectively.

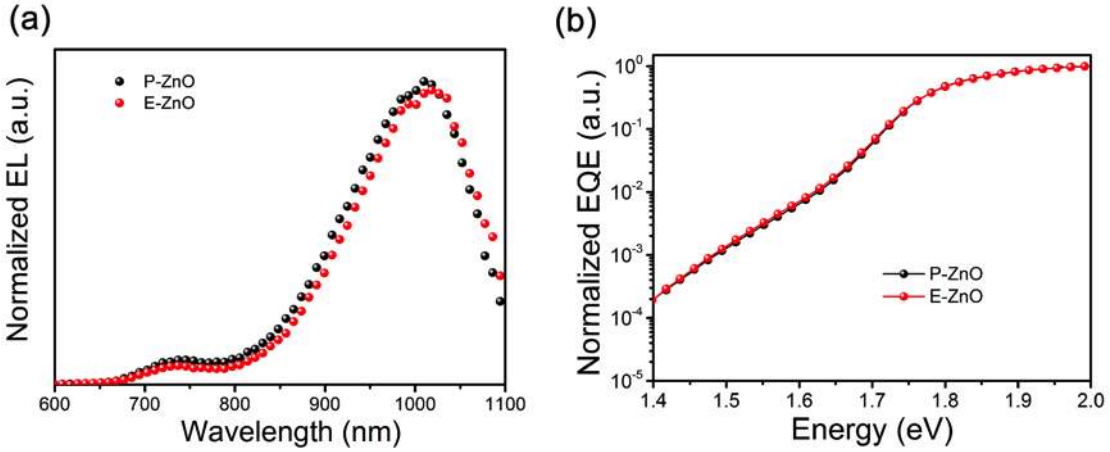

Figure S9. Normalized EL (a) and FTPS spectra (b) from inverted TQ1:$PC_{71}BM$ devices based on P-ZnO ETLs and E-ZnO ETLs, respectively.

References:

[1] L. A. A. Pettersson, L. S. Roman, O. Inganas, *J. Appl. Phys.* **1999**, 86, 487-496.
[2] C. M. Ramsdale, N. C. Greenham, *J. Phys. D: Appl. Phys.* **2003**, 36, L29.
[3] H. Hoppe, N. S. Sariciftci, D. Meissner, *Molecular Crystals and Liquid Crystals* **2002**, 385, 113-119.
[4] S. Shao, J. Liu, J. Bergqvist, S. Shi, C. Veit, U. Würfel, Z. Xie, F. Zhang, *Adv. Energy. Mater.* **2013**, 3, 349-355.